Chapter 5

Collisions and loss in a Rb-Cs MOT

The MOT has been described as the 'workhorse' of atomic physics [202]. As such, achieving a MOT is frequently regarded as a step on the road to quantum degeneracy or more complex experiments rather than as an end in itself. The experimental apparatus described in the previous chapter, for example, is currently being used to study Rb-Cs mixtures at temperatures much colder than the $\sim$100 μK achievable in the two-species science MOT. Yet this picture of a MOT as a means to an end ignores two important facts. Firstly, despite almost two decades of experimental and theoretical work (see *e.g.* Refs. [96, 141] and references therein), the atom-light and atom-atom interactions taking place in a 3D MOT are still not fully understood. Secondly, the flip side of being an unglamorous workhorse is that a good MOT is the *sine qua non* of many experiments: having fewer atoms in the MOT means fewer atoms available for transfer into magnetic or optical traps, making it more difficult to reach quantum degeneracy via evaporative cooling.

Part of Chapter 3 was devoted to a discussion of the cold collisions which lead to a loss of atoms from one- and two-species MOTs. Such information is needed to understand the measurement methods used in our studies of the Rb-Cs MOT, the dependence of loss on MOT parameters like intensity, gradient and detuning, and the special challenges of two-species MOTs. Experimentally, however, our primary focus was not on the specific loss processes but on how we could reduce or suppress them and thus increase the

number of cold Rb and Cs atoms available for loading into the magnetic trap. The bulk of this chapter is therefore devoted to experimental measurements of MOT loss.

5.1 Introduction

Since the first demonstration of a two-species MOT of ^{87}Rb and ^{85}Rb in 1994 [203], a number of different mixture MOTs have been studied experimentally. These include MOTs containing various combinations of alkali metal atoms (see *e.g.* Ref. [65] and references therein), rubidium and metastable argon [204], and rubidium and chromium atoms [66]. Recently, a three-species MOT of rubidium and fermionic isotopes of lithium and potassium has also been demonstrated [205].

Several topics appear repeatedly in the experimental literature on two-species MOTs. The most common experiments study the loss of one species from the MOT in the presence and absence of a second trapped species. This allows the relative contributions of single-species and two-species inelastic collisions to the total loss rate to be determined. We present the results of such loss measurements on our Rb-Cs MOT in Section 5.2. A common extension is to examine how the loss rates vary with the intensity [206] or detuning [207] of the trapping beams. We saw in Chapter 3 that many of the MOT loss mechanisms depend on intensity, detuning, or both. Hence, information on intensity or detuning dependence of loss can indicate which loss mechanisms are most important for a particular species or set of experimental conditions. Numerous studies of single-species MOTs [141] have found that relatively small alterations in trap parameters, *e.g.* a factor of two change in intensity, can produce changes of several orders of magnitude in the loss rate coefficients.

A less common type of experiment attempts to separate the contributions of different loss channels to the total loss rate. This was done for lithium and caesium by chopping the Li trapping light, thereby altering the average excitation of the Li atoms [75]. It is also possible to gain information about different loss channels by measuring the rate at which atom-ion molecules are produced in the MOT, using a time-of-flight spectrometer [208]. Such

measurements were beyond the scope of this work, and are mentioned chiefly to provide some idea of experiments which can be performed to understand the MOT loss mechanisms discussed theoretically in Chapter 3.

5.2 Measurement methods

We now turn away from a general discussion of two-species MOTs to examine how the single-species and two-species loss rate coefficients can be measured. It is helpful to recall from Chapter 3 that the time-evolution of a single-species MOT is described by the rate equation

$$\frac{dN_i}{dt} = L - \gamma N_i - \beta_i \int n_i^2 d^3r, \tag{5.1}$$

while the two-species equation is

$$\frac{dN_i}{dt} = L - \gamma N_i - \beta_i \int n_i^2 d^3r - \beta_{ij} \int n_i n_j d^3r. \tag{5.2}$$

Three methods have been used to measure values of β and thereby characterise MOT loss. The first of these examines the MOT as it is being loaded and is included here for completeness as it was not used in our studies. The other two methods were used, and are described in more detail.

5.2.1 Loading method

Assuming the MOT loads at a constant density [209], the one-species equation reduces to

$$\frac{dN_i}{dt} = L - (\gamma + \beta_i \langle n_i \rangle) N_i, \tag{5.3}$$

where $\langle n_i \rangle$ is the mean number density and we have considered only one-species MOTs for simplicity. The factor $\gamma + \beta_i$ is determined by measuring the number of trapped atoms as a function of time, *e.g.* by recording the fluorescence with a photodetector. Solutions to Eq. 5.3 are then fit to the data. Figure 5.1 shows the loading of the Cs MOT after the repumping beam is unblocked at $t = 0$. In order to extract β_i, a separate experiment must be performed in which the MOT is operated at very low atom numbers. In this regime, cold collisions play little role in the total loss rate, and the equation reduces further to

$$\frac{dN_i}{dt} = L - \gamma N_i. \tag{5.4}$$

This allows γ to be measured independently. If we assume that $\gamma \approx 0$ for the data in Figure 5.1, and take the cloud density to be 4.29×10^9 cm^{-1} (the average value for all Cs clouds, measured from absorption images), a fit to the loading curve for $t = 0 - 40$ s gives $\beta_{\mathrm{Cs}} = 4.65(9) \times 10^{-11}$, where the error is calculated from the fit.

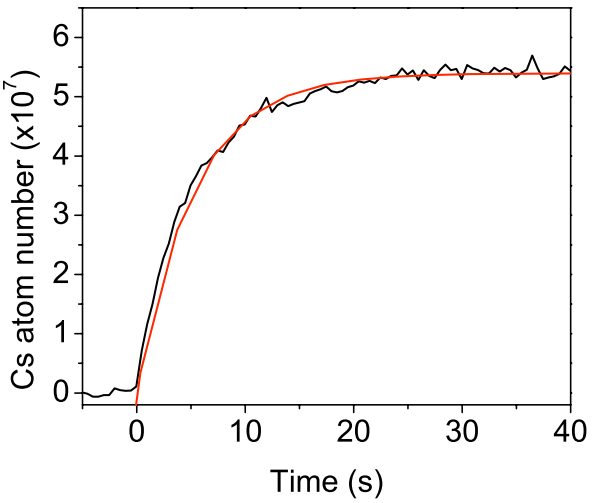

Figure 5.1: Loading of the single-species Cs MOT. Unblocking the repumping beam at $t = 0$ allows Cs atoms to be trapped in the science MOT. The loss rate coefficient β_{Cs} can be determined by fitting Eq. 5.3 to the data.

5.2.2 Decay method

A second technique allows the values for β_i and γ to be measured in a single experimental run. In this method, the loading is turned off ($L = 0$ in Eqs. 5.1 and 5.2) and the fluorescence observed as the MOT decays. Initially, the decay occurs in a constant density regime, where the MOT loses atoms and decreases in size without any change in density. Later, the density begins to decrease. Eventually, the density is so low that collisions with the background gas are the dominant loss mechanism. As the decay of one species can be recorded either in the presence or absence of a second species, this method can be used to measure both single-species and two-species loss rate coefficients.

For decays of two-species MOTs, the two-species rate equation becomes

$$\frac{\mathrm{d}N_i}{\mathrm{d}t} = -\left(\gamma + \beta_i\langle n_i\rangle + \beta_{ij}\langle n_j\rangle F_{ij}\right) N_i, \tag{5.5}$$

where the factor F_{ij} represents the (normalised) density of species j weighted by the probability distribution of species i. F_{ij} approaches zero as the two clouds become spatially separated, while two clouds of equal size centred at the same position will have an F_{ij} of unity. F_{ij} may therefore be thought of as a measure of the relative overlap of the two trapped atom clouds.

5.2.3 Steady-state method

The third method is specific to two-species MOTs. In the so-called 'steady-state' method, the interspecies rate coefficients are determined by comparing equilibrium values of atom number and the size of trapped clouds in the single-species MOT to the corresponding equilibrium values with another species present. In this method, Eq. 5.2 is solved for β_{ij} in the presence and absence of a second species. To do this, we recall that the average densities for single and two-species atom clouds are defined as

$$\begin{aligned}\langle n_i\rangle &= \frac{1}{N_i}\int n_i^2 d^3r \\ \langle n_{ij}\rangle &= \frac{1}{N_i}\int n_i n_j d^3r.\end{aligned} \tag{5.6}$$

Using these definitions, the rate equation becomes

$$\frac{dN_i}{dt} = L - \gamma N_i - \beta_i\langle n_i\rangle N_i - \beta_{ij}\langle n_{ij}\rangle N_i. \tag{5.7}$$

These definitions also allow us to formally define the 'overlap' factor F_{ij} as

$$F_{ij} = \frac{\int n_j n_i/N_i d^3r}{\int n_i n_i/N_i d^3r} = \frac{\langle n_{ij}\rangle}{\langle n_i\rangle}. \tag{5.8}$$

To obtain an expression for β_{ij}, steady-state solutions to the rate equation are found in the presence and absence of a second species. In the single-species MOT, this gives

$$L = \gamma\tilde{N}_i + \beta_i\langle\tilde{n}_i\rangle\tilde{N}_i, \tag{5.9}$$

where the $\tilde{}$ denotes quantities in the single-species MOT. Adding a second species changes the equation to

$$L = \gamma N_i + \beta_i\langle n_i\rangle N_i + \beta_{ij}\langle n_{ij}\rangle N_i. \tag{5.10}$$

Solving for β_{ij} gives the result:

$$\beta_{ij} = \frac{1}{\langle n_{ij} \rangle N_i} \left[\gamma \left(\tilde{N}_i - N_i \right) + \beta_i \left(\langle \tilde{n}_i \rangle \tilde{N}_i - \langle n_i \rangle N_i \right) \right]. \tag{5.11}$$

5.3 Modifications to experimental setup

All of the methods for measuring β_i and β_{ij} require knowledge of the number of atoms in the MOT and their density profile to calculate the loss rate coefficients. Fluorescence detection allows changes in atom number to be observed in real time, and is thus essential for decay or loading measurements. The steady-state atom number can be obtained either from fluorescence detection or via absorption images. Absorption images provide information about the atoms' location (important for calculating the overlap between trapped Rb and Cs atoms) and the cloud density. This section describes modifications to the diagnostic systems and to the optimum MOT parameters which were made specifically for the MOT measurements.

5.3.1 Fluorescence measurements

In order to monitor MOT decay, we needed to record the evolution of the atom number for longer than the 100 s maximum period for a single oscilloscope scan. The fluorescence detection system used for the MOT measurements was therefore modified from the standard setup used for routine diagnostics. The signals from the two fluorescence photodiodes were first sent to a pair of current-to-voltage converter circuits (Figure 5.2). The circuits allowed us to monitor the photodiode signal on the oscilloscope and a GPIB-enabled volt meter at the same time, without any change of signal due to problems with impedance matching the two devices. The circuit also featured four gain settings, which are summarised in Table 5.1. The gain factors were calibrated using a constant light source and are within 10% of their expected values based on the resistors used. Both battery-powered and mains-powered circuits were constructed; however, only the mains-powered circuits were used in these experiments.

In the description of the fluorescence detection apparatus in Chapter 4, it was noted that the dichroic mirror reflects a small percentage of the Rb

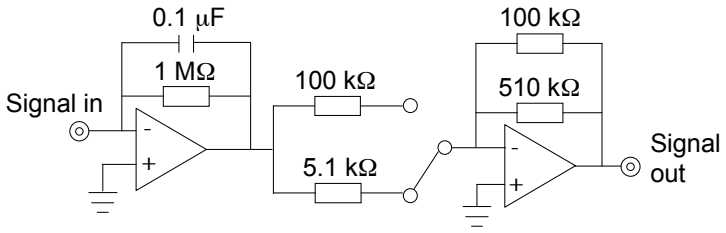

Figure 5.2: Current-to-voltage converter circuit. The signal from the fluorescence photodiode is sent through this circuit before being recorded on an oscilloscope and a digital voltmeter. AD648 op-amps were used for the battery powered circuit, while a mains-powered version used TL082s.

Resistor 1	Resistor 2	Expected gain	Measured gain
100 kΩ	100 kΩ	× 1	× 0.944(8)
100 kΩ	510 kΩ	5.1	4.9(2)
5.1 kΩ	100 kΩ	19.6	18.8(8)
5.1 kΩ	510 kΩ	100	95(7)

Table 5.1: Predicted and measured gain settings for current-to-voltage converter circuit.

light onto the photodiode monitoring Cs fluorescence. The effect of this on the Cs fluorescence signal is shown in Figure 5.3. The red (black) curve is the Rb (raw Cs) fluorescence signal. At $t = 25$ s, the Rb repumping light was unblocked and the Rb MOT began to fill. The signal recorded by the photodiode monitoring Cs light increased proportionally to the Rb signal until $t = 200$ s, when the Cs repumping light was unblocked. The sharp jump in the black curve represents the presence of actual Cs fluorescence. This problem was solved by subtracting a percentage of the Rb signal from the raw Cs signal. The amount of the correction was empirically set to 1.2(2)%, the value which gave a flat Cs signal in the absence of a Cs MOT. This is shown in the blue curve in Figure 5.3.

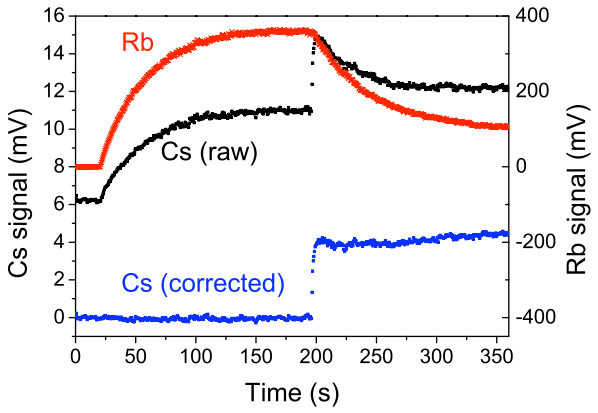

Figure 5.3: Effect of leaked Rb light on Cs fluorescence signal. The red curve shows Rb fluorescence as the MOT loads, starting at $t = 25$ s. The black curve shows the raw Cs fluorescence signal, which mirrors the Rb curve until $t = 200$ s, when the Cs MOT was turned on. The blue curve shows the Cs signal after 1.2% of the Rb signal was subtracted from the raw Cs signal.

5.3.2 Absorption imaging in the MOT

Imaging in the MOT was performed with the CCD camera in bulb mode. In this mode charge is being continuously drained away from the CCD whenever the camera is not firing. In theory this means that any light which falls on the camera before the image is taken will not affect the image. In practice the time required to remove charge depends on the amount of light which has fallen on the camera. For our system, images taken less than ∼30 ms after the MOT light has been switched off contain images of MOT fluorescence in addition to the intended absorption image. This leads to the optical depths being underestimated, because the probe and background images do not contain residual MOT fluorescence. This is not a problem for imaging in the magnetic trap, because the atoms are typically held in the trap for $\gg 100$ ms before the images are taken. For MOT imaging *in situ* it was necessary to modify the standard imaging sequence to allow the unwanted fluorescence to be subtracted. The new imaging sequence is:

1. Image a: absorption + probe + fluorescence + background

2. Image b: probe + background
3. Image c: background only
4. Image f: fluorescence + background.

Image f is obtained during a separate data run, during which the probe beam is blocked during the imaging cycle. The new, corrected Image A which is imported by the Matlab code for analysis is

$$\mathrm{A} = \mathrm{a} - \mathrm{f} + \mathrm{c}. \tag{5.12}$$

Figure 5.4 contains absorption and fluorescence images of the MOT. As discussed in Chapter 4, the images show an array of optical depths, with higher depths shown in red. Note that the fluorescence appears as a negative optical depth; hence, optical depths in the corrected Image A will be higher than in the uncorrected version.

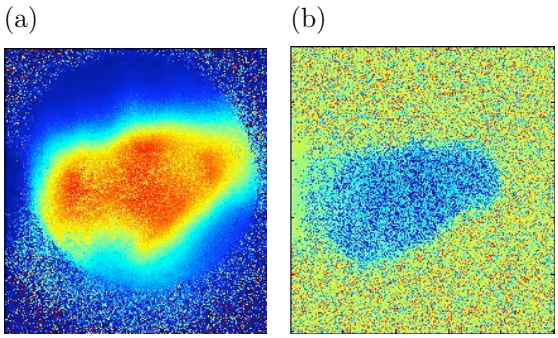

Figure 5.4: (a) Absorption+probe+fluorescence+background and (b) fluorescence+background images of the Rb science MOT. The fluorescence image is subtracted from the absorption image during image processing.

5.3.3 MOT parameters

Very large MOTs presented a challenge for absorption imaging. The largest Rb MOTs we measured nearly filled the camera's field of view along the radial direction, even after we reduced the magnification of the imaging system from $\sim$1 to 0.46(5). Our solution to this (happy!) problem was to increase the

	^{87}Rb	^{133}Cs
Pyramid MOT detuning (Δ/Γ)	-2.80(3)	-3.06(4)
Science MOT detuning (Δ/Γ)	-1.99(3)	-3.49(4)
I_{Pyramid} (mW cm^{-2})	49.2(6)	49.8(8)
I_{Science} (mW cm^{-2})	11.0(3)	11.8(3)
MOT gradient (G cm^{-1})	20.8(2)	20.8(2)

Table 5.2: Summary of experimental parameters during the MOT measurements. The natural linewidth Γ is $2\pi\times6.06$ MHz ($2\pi\times5.22$ MHz) for Rb (Cs). The MOT intensities represent values due to all the beams combined.

magnetic field gradient to 20.8(2) Gcm^{-1}. This compressed both MOTs, and also ensured that the Cs MOT was located entirely within a larger Rb MOT — an effect desirable in its own right. The detuning of the Cs MOT was also changed to $\Delta/\Gamma = -3.49(4)$ to increase the number of trapped Cs atoms at the higher gradient. All other MOT parameters remained at their optimum values given in Chapter 4; Table 5.2 provides a full list of parameters.

At the new gradient and Cs MOT detuning, the increased density of the clouds meant that the measured optical depths for all but the smallest Cs clouds were very high (> 3.5). At such high optical depths, a very small increase in the absorption produces a disproportionately large increase in the optical depth. Taken at face value, such measurements would lead us to overestimate the number of atoms in the MOT. To avoid this, we performed all of our absorption imaging with the Cs probe beam detuned from resonance. The densities derived from the optical depth were then corrected for the detuning. Studies of detuned and resonant imaging in both species showed very similar results for the cloud radii regardless of the probe detuning.

5.4 Single-species loss measurements

We used the decay method to measure the single-species loss rate coefficients β_{Rb} and β_{Cs}. Figure 5.5 shows the fluorescence of the Rb MOT after the Rb pyramid MOT beam was blocked with a shutter. The decay is plotted on a logarithmic scale, so that periods of exponential decay are indicated by straight lines in the data. Initially, the decay occurs at a constant density

and the rate is exponential. As the number of atoms decreases, the radiation absorption effect of the MOT weakens enough that further loss of atoms results in a decrease in density, and the rate of loss increases. The density distribution of the cloud becomes Gaussian during this period. Eventually, the cloud enters the regime where cold collisions are no longer a major loss mechanism, as discussed in Chapter 3. The loss rate is again exponential, but with a reduced time constant γ determined by background gas collisions. Measurements of both species' lifetime in the magnetic trap showed that $\gamma = 1.5(3) \times 10^2$ s.

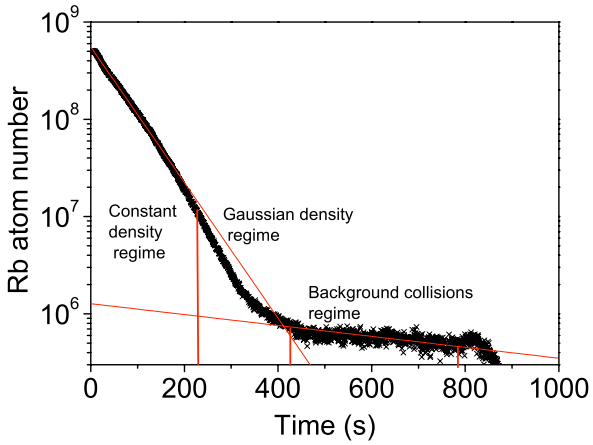

Figure 5.5: Fluorescence signal recorded during decay of Rb MOT. Initially, the density of the atom cloud remains constant and the MOT decays exponentially (first region). At some point, the density begins to decrease, and the decay is no longer exponential (second region). Eventually, so few atoms are left in the MOT that cold collisions play little role, and the decay is again exponential (third region).

We want to extract our values for β_{Rb} and β_{Cs} from the period in which the density is constant and limited by the re-radiation of photons discussed in Chapter 3. The precise boundaries of this period are not clear from the decay curves alone. To clarify the extent of the constant-density regime, a series of absorption images was taken for several different numbers of trapped atoms. The densities derived from these images showed considerable variation for MOTs containing less than $\sim 10^6$ atoms, and we have already noted that

very large MOTs ($> 5 \times 10^8$ atoms) are difficult to image. At intermediate values, the densities were relatively constant. This is illustrated in Figure 5.6 (a). Note that the magnitudes of the densities in this figure are lower than for most MOTs we studied by approximately a factor of 1.7; this is because these data were taken during preliminary experiments at the lower (optimised) gradient of 10.8 Gcm^{-1}. Later experiments at the higher gradient of 20.8 Gcm^{-1} focused on imaging only Rb MOTs in the constant-density regime, as shown in Figure 5.6 (b).

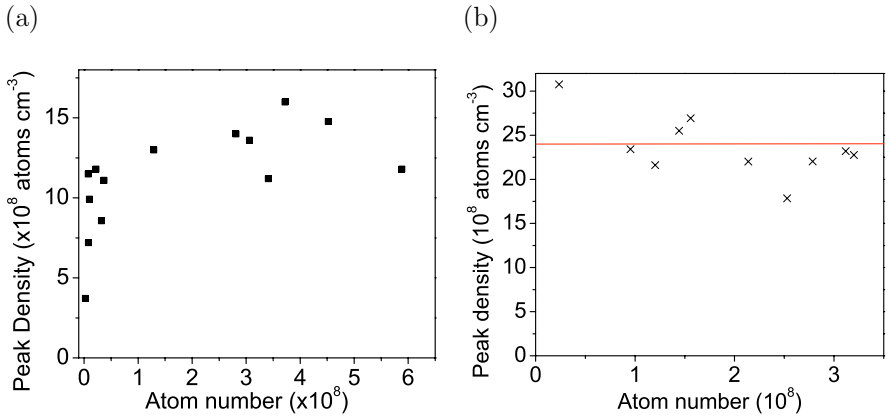

Figure 5.6: (a) Peak density of the Rb MOT as a function of atom number at a magnetic field gradient of 10.8 Gcm^{-1}. For MOTs containing more than $\sim 10^8$ atoms, the density is relatively constant. (b) Similar data taken at the higher gradient of 20.8 Gcm^{-1}, this time focusing only on the constant-density regime. The red line shows the mean value for the data set of $2.4(1)\times10^9$ atoms cm^{-3}. The intensity and detuning of the MOT light was the same for both figures, with values given in Table 5.2.

Further evidence that the MOT is decaying exponentially for this atom number range was obtained by performing a series of fits to the decay curve in Figure 5.5. Each point in Figure 5.7 represents the value of $\tau = 1/(\beta_{\mathrm{Rb}} n_{\mathrm{Rb}})$ measured by fitting an exponential to 20 s of decay. Between 20-280 s, corresponding to $\sim 56 - 0.56 \times 10^7$ Rb atoms, τ is constant to within 15%. The sharp increase in τ after 300 s indicates a change in the MOT behaviour, and the increase in the size of the error bars indicates that the decay is not well approximated as exponential. We conclude that at this point, the MOT

has entered the non-constant density regime. Similar data for Cs showed that the decay of the Cs MOT is exponential for the first 20 s, corresponding to $\sim 0.36 - 7 \times 10^7$ Cs atoms.

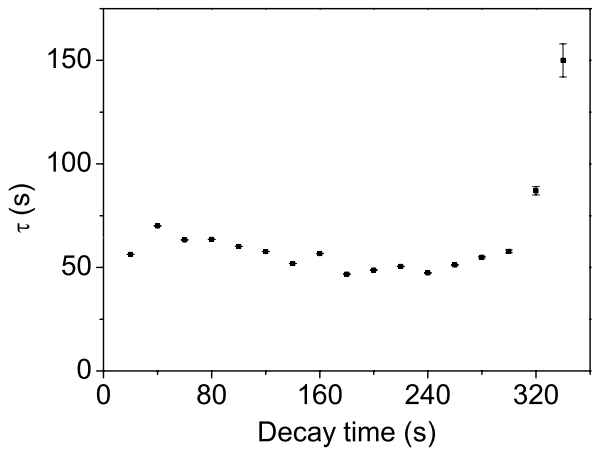

Figure 5.7: A series of fits to the decay curve in Figure 5.5 shows that the time constant $\tau = 1/(\beta_{\mathrm{Rb}} n_{\mathrm{Rb}})$ of the decay varies little for the first 300 s. The sharp increase near that time indicates a change in decay behaviour; larger error bars indicate that the decay is no longer exponential.

Single exponential fits to the Cs and Rb decay data over these time periods yielded $\beta_{\mathrm{Rb}} = 1.5(2) \times 10^{-11}\mathrm{cm}^3\mathrm{s}^{-1}$ and $\beta_{\mathrm{Cs}} = 2.1(1) \times 10^{-11}$ cm $^3\mathrm{s}^{-1}$, where the errors represent statistical variation over four decay measurements per species. Additional systematic uncertainties of up to 30% arise primarily from measurements of atomic cloud sizes. These values are in good agreement with the available published data [210, 211].

5.5 Two-species loss measurements

We first measured the two-species rate constants β_{RbCs} and β_{CsRb} by comparing the decay rates of Rb and Cs (in the constant-density regime) in the presence and absence of a second species. The MOTs were initially loaded to their two-species equilibrium values. The Cs pyramid MOT beam was then switched off, and the Cs MOT allowed to decay in the presence of cold Rb.

Although the number of Rb atoms increased during this decay, the position of the Cs MOT near the centre of the much larger Rb cloud meant that the overlap factor F_{CsRb} remained constant, and the Cs decay curve could be described by a single exponential throughout the density-limited regime. As Figure 5.8(a) shows, the Cs MOT lifetime is reduced by a factor of five from the single-species value in the presence of Rb. Averaging over three decay curves yielded $\beta_{\mathrm{CsRb}} = 1.0(6) \times 10^{-10}\mathrm{cm}^3\mathrm{s}^{-1}$.

To measure β_{RbCs} using the decay method, we restricted our fit to the first 10 s. Shortly after this period, the Cs atom number started to increase, and the Rb decay accelerated as a larger fraction of the Rb cloud was in contact with cold Cs. Figure 5.8(b) illustrates this. Measurements of initial Rb decay in the presence of Cs yielded $\beta_{\mathrm{RbCs}} = 1.6(4) \times 10^{-10}\mathrm{cm}^3\mathrm{s}^{-1}$.

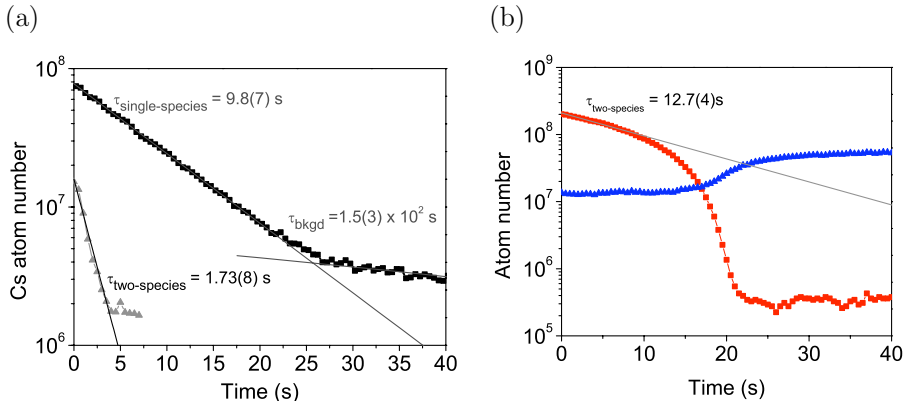

Figure 5.8: (a) Decay of the Cs MOT in the presence (grey) and absence (black) of cold Rb. The presence of the Rb MOT reduces the Cs MOT lifetime by a factor of five due to light-assisted interspecies inelastic collisions. (b) Decay of the Rb MOT (red) in the presence of the Cs MOT (blue). After ∼10 s of exponential decay, during which time the number of Cs atoms is nearly constant, the recovery of the Cs MOT produces an acceleration in the Rb decay rate.

We also characterised the two-species loss rates using the steady-state method. Figure 5.9 shows a typical loading sequence used to extract the number of atoms present in the single-species and two-species equilibria. Initially, no repumping light is present, preventing the MOTs from forming. At

$t = 0$ s, the Cs repumping beam is unblocked, and the Cs MOT loads to its single-species equilibrium level. At $t = 45$ s the Rb repumping beam is unblocked, and collisions with cold Rb atoms cause rapid losses of $\sim 75\%$ of the trapped Cs atoms. The loading sequence is then reversed. Absorption images were taken of the Cs and Rb MOTs at their single-species and two-species equilibrium levels and values for the cloud radii obtained from Gaussian fits to these images. Figure 5.10 shows typical images of the single-species and two-species Rb and Cs MOTs. Note that in the two-species MOT, the Cs atom cloud is located entirely inside the Rb cloud. Hence, the Cs MOT decays very rapidly in the presence of Rb, whereas the Cs MOT simply acts like a small 'hole' in the Rb MOT, and its presence causes less rapid loss of Rb.

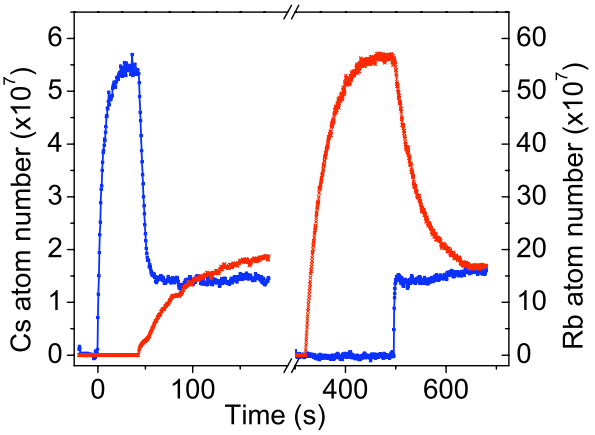

Figure 5.9: Sample sequence for steady-state measurements showing loading and loss in the Rb-Cs MOT. Initially, only Cs (blue line) is trapped. Unblocking the Rb repumping beam after 45 s leads to rapid losses of $\sim$75% in the Cs cloud. At $t = 300$ s the loading sequence is reversed. Note that the Cs MOT reaches its two-species equilibrium value within 10 s after the Cs repumping beam is unblocked, while the Rb cloud decays much more slowly due to the reduced overlap with the Cs cloud.

Based on these steady-state measurements, we found $\beta_{\mathrm{RbCs}} = 2.1(3) \times 10^{-10}$ cm^{3}s^{-1} and $\beta_{\mathrm{CsRb}} = 9(2) \times 10^{-11}$ cm^{3}s^{-1}, where the errors represent statistical variation over 3 (4) data sets for β_{RbCs} (β_{CsRb}). Additional systematic

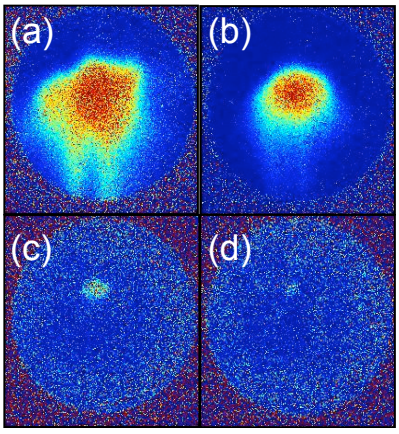

Figure 5.10: Absorption images of Rb and Cs in the single-species and two-species MOTs. Images of the Rb cloud without (a) and with (b) Cs present show a sharp reduction in cloud size due to interspecies inelastic collisions. Similar images of the Cs MOT without (c) and with (d) Rb present also show equilibrium numbers much reduced in the two-species MOT.

uncertainties of up to 30% arise primarily from measurements of atomic cloud sizes. These values are in good agreement with the values from the decay measurements.

5.6 Minimising interspecies loss

The very strong interspecies loss evident from both measurements presents a challenge for optimising the two-species Rb-Cs MOT. One possible optimisation strategy would be to alter the alignment and intensity balance of the MOT beams from their single-species optimised values in order to reduce the overlap of the two clouds. This realignment can be time-consuming, and ultimately one wants the two clouds well overlapped in order to load both into the centre of the magnetic trap. Additionally, changing the detunings and intensity of the MOT beams can in some cases be beneficial. Gensemer *et al.* demonstrated that for Rb, shifting the laser detuning by just one natural linewidth can change β_{Rb} by up to three orders of magnitude [210]. However, as Weiner *et al.* have discussed, the relationship between detuning, intensity,

and trap loss rate is quite complex even for single-species MOTs [141]. The parameter space is thus very large, and it is difficult to know *a priori* what effect changes will have on the loss rate.

We have developed an alternative method for reducing the interspecies loss which does not require any deviation from the optimum single-species MOT parameters. In this technique, a beam of light (with a $1/e^2$ radius of 7(1) mm and a peak intensity of $0.48(2)\,\mathrm{mWcm^{-2}}$) close to resonance with the Rb cooling transition is aligned through the MOT centre during loading. The effect is to shift the centre of the Rb MOT by several mm, spatially separating the trapped Rb and Cs clouds. This 'push' beam is simply the beam used for absorption imaging at a higher intensity. Implementing the displaced MOT thus requires no additional optics or alignment. Optimum conditions for single-species trapping can be recovered by turning off the push beam, with no need for complex and time-consuming adjustments.

Figure 5.11(a) shows the fluorescence of the Rb and Cs MOTs during loading with and without the Rb MOT displaced. The Rb MOT is allowed to load to approximately 50% of its maximum single-species level before the Cs MOT loading is turned on at $t = 40$ s. With the push beam off, the Cs MOT loading is strongly suppressed, and the Rb MOT begins to decay. When the experiment is repeated with the push beam on, the Rb MOT loading proceeds unimpeded, and the Cs MOT reaches $\sim 70\%$ of its single-species level before the Rb and Cs clouds begin to overlap, and interspecies inelastic collisions prevent further increase in the Cs atom number. If necessary, the overlap could be reduced further by displacing the Cs MOT as well. Using the displaced MOT technique, we have created two-species Rb-Cs MOTs containing a total of more than 10^9 atoms.

The effect of the displaced MOT technique on the magnetic trap loading is also pronounced. At the end of the MOT loading phase, a standard sequence of CMOT, optical molasses and optical pumping is used to load the atoms into the magnetic trap, as described in Chapter 4. The push beam is switched off immediately before the start of the CMOT phase, so that the two trapped atomic clouds become well overlapped prior to loading the magnetic trap. The short duration of the loading phase, however, means that there are no detectable losses due to interspecies light assisted collisions even though the

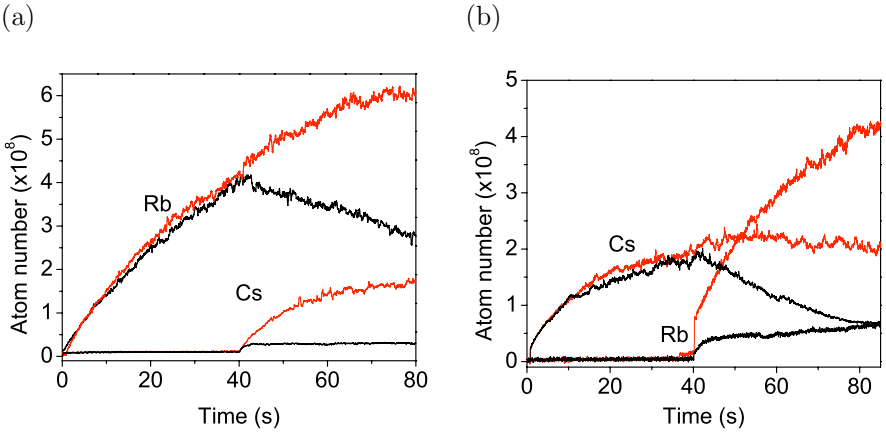

Figure 5.11: Performance of the displaced double MOT. (a) The Cs MOT is switched on after 40 s of loading Rb alone. Without the push beam (black line), atoms are lost from the Rb MOT due to light assisted interspecies inelastic collisions, and loading of the Cs MOT is greatly impaired. Turning the push beam on (red line) displaces the Rb MOT from the Cs MOT loading region, limiting losses due to interspecies collisions. (b) A similar sequence, but with Cs loaded first. With the push beam on (red lines), the Cs MOT reaches $\sim 70\%$ of its single-species level before being limited by the presence of the Rb MOT. The Rb MOT loading proceeds unimpeded with the push beam on, but is greatly impeded in the non-displaced MOT (black line).

clouds are well overlapped at this stage.

Figures 5.12(a)–(c) contain images of magnetically trapped clouds taken with and without the push beam on during the MOT phase. The figures also contains vertical cross-sections of the atom clouds, showing the increase in optical depth for magnetically-trapped atoms loaded from the displaced MOT. The flexibility of the displaced MOT technique allows us to vary the composition of the trapped mixture over a wide range by adjusting the load duration of each species. We can load mixtures containing an equal amount of each species at close to their respective maximum single-species atom numbers. At the other extreme, we can load one species to its single-species maximum together with an arbitrarily small amount of the second species.

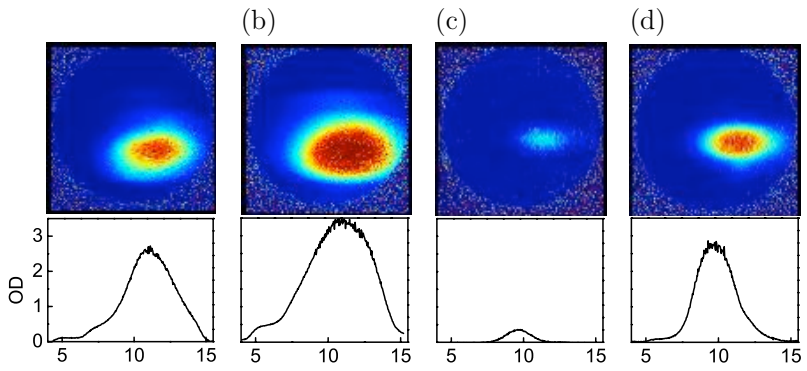

Figure 5.12: Absorption images of magnetically trapped Rb clouds loaded from unperturbed (a) and displaced (b) MOTs. Cross sections of the clouds in the vertical direction show increases in optical depth and size with the push beam present. Similar images of Cs clouds without (c) and with (d) the Rb MOT displaced show even more significant improvement. All images are displayed on an optical depth scale of 0-3 except the unperturbed Cs cloud, which is on a 0-1 scale. The cross sections are on a common 0-3.5 scale.

5.7 Conclusions

In summary, measurements on the Rb-Cs science MOT showed strong losses due to light-assisted inelastic collisions between the two species. For our MOT parameters, the rate coefficients β_{RbCs} and β_{CsRb} for two-species loss are approximately one order of magnitude larger than the single-species loss coefficients. This indicated that reducing two-species loss would lead to significant improvements in MOT performance. A simple but effective technique was developed to suppress two-species collisions by spatially separating the Rb and Cs MOTs during loading. This method is not specific to the Rb-Cs mixture, and should prove useful in reducing loss in other two-species MOTs.

The work on MOT losses described in this chapter was essential to the future progress of the Rb-Cs mixture experiment. The knowledge gained about the MOT has given us a better understanding of optimum loading conditions for the two-species MOT. In particular, the displaced MOT technique has proved a reliable and consistent method of preparing atoms for loading into

the magnetic trap. A particular advantage is that the push beam technique allows considerable flexibility in the ratio of Rb to Cs atoms available for loading into the magnetic trap. The two-species MOT we have developed thus represents an advantageous starting point for a range of experiments on cold Rb-Cs mixtures, including a search for interspecies Feshbach resonances and studies of sympathetic cooling.